Open

ORIGINAL ARTICLE

Non-locality and collective emission in disordered lasing resonators

Marco Leonetti[1,2], Claudio Conti[1,3] and Cefe Lopez[2]

Random lasing is observed in optically active resonators in the presence of disorder. As the optical cavities involved are open, the modes are coupled, and energy may pour from one state to another provided that they are spatially overlapping. Although the electromagnetic modes are spatially localized, our system may be actively switched to a collective state, presenting a novel form of non-locality revealed by a high degree of spectral correlation between the light emissions collected at distant positions. In a nutshell, light may be stored in a disordered nonlinear structure in different fashions that strongly differ in their spatial properties. This effect is experimentally demonstrated and theoretically explained in titania clusters embedded in a dye, and it provides clear evidence of a transition to a multimodal collective emission involving the entire spatial extent of the disordered system. Our results can be used to develop a novel type of miniaturized, actively controlled all-optical chip.

INTRODUCTION

Non-locality plays a fundamental role in various areas of applied science, such as plasma physics and Bose–Einstein condensation.[1–3] In nonlinear optics, non-locality is usually associated with photorefractive, thermal or elastic responses.[4–8] In this letter, we demonstrate the signature of non-locality in an active disordered optical system:[9,10] a random laser (RL).[11]

RLs are among the most complex systems in photonics, encompassing structural disorder, nonlinearity,[12] strong nonlinear interaction[13] and different photon statistics[14] in systems ranging from micron-sized optical cavities[15] to kilometer-long fibers.[16] First-principles time-domain simulations show that the modes of a RL arise from localized electromagnetic states,[17–19] which may appear in a localized or an extended fashion. Several experiments have been reported on the nature of these modes,[15,20–22] and these studies attempted to address the correlation between the structure and the degree of localization.

Recently, it has been experimentally demonstrated that controlling the shape of the population-inverted area and thus the directionality of the amplified spontaneous emission of the dye in the area surrounding the lasing cluster (Figure 1a) makes it possible to affect the number of activated modes and their degree of interaction.[23] Such control is possible for a system composed of an individual micrometer-sized cluster of titanium dioxide nanoparticles lying in a bath of a rhodamine-doped solution. By pumping the area surrounding the cluster, one can generate a flux of directional stimulated emission capable of pumping only modes that are well coupled with the pump shape, and the lasing threshold may be surpassed (Figure 2). The number of activated modes is controlled by selecting, through a spatial light modulator, the angular aperture Θ of the wedge-shaped pumped area (see Figure 1b and studies[23–25] for further details).

In this way, it is possible to drive the RL between two intrinsically distinct regimes, distinguished by the shape of the spectral emission: a 'resonant feedback random laser',[26] which appears as a set of sharp peaks oscillating independently at fixed spectral positions, and an 'intensity feedback random laser' or 'incoherent feedback random laser',[27] characterized by a smooth, single-peaked spectrum which appears line-narrowed with respect to the fluorescence. A resonant feedback random laser is observed when activating a typically small set of weakly interacting resonances, while an incoherent feedback random laser is produced under strong interaction that leads to a mode-locked synchronized regime.

A striking and unexpected phenomenon is found if one studies the spatial properties of the individual lasing modes. Extended modes are favored in the highly interacting regime, while local resonances are activated in the barely interacting configuration.[25] Here, we will demonstrate that the change in the mode shape with Θ for a fixed disorder is due to a novel form of non-locality mediated by the mode-coupling between the open cavities constituting the set of involved resonators.[17,28] To date, spatial non-locality has been largely investigated in Hamiltonian nonlinear optical systems, but here we report the first evidence in a dissipative disordered medium.

MATERIALS AND METHODS

The experiments were performed on individual clusters obtained through an isolation procedure from titanium dioxide powder titanium dioxide (titanium(IV) oxide, 89490 Sigma-Aldrich, particle

[1]ISC-CNR, UOS Sapienza, 00185 Roma, Italy; [2]Institute for Material Science Madrid (ICMM-CSIC), 28049 Madrid, Spain and [3]Department of Physics, University Sapienza, I-00185 Roma, Italy
Correspondence: Dr M Leonetti, ISC-CNR UOS, La Sapienza, Piazzale Aldo Moro 5, 00185 Roma, Italy
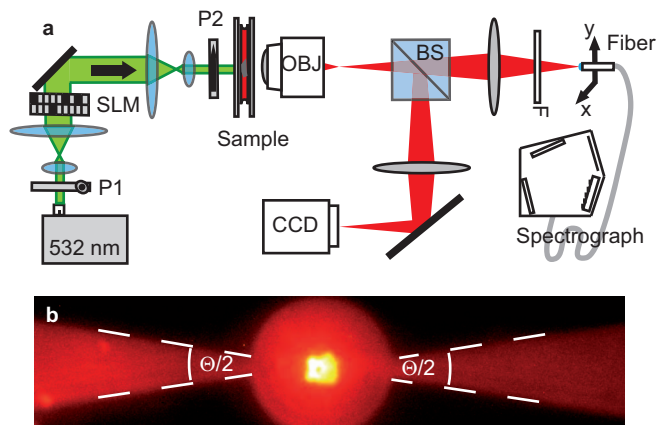E-mail: marco.leonetti@roma1.infn.it

2

Figure 1 (**a**) Experimental set-up. Laser light from a Nd:YAG frequency doubled pulsed laser is shaped from a reflective spatial light modulator to generate a population-inverted area of the shape indicated in **b**. Light emitted from the sample is collected from an OBJ and imaged through a BS on a CCD camera and on a plane in which a motor-controlled fiber is placed. The fibers collect only light emitted from a region much smaller than the cluster, thus eliminating contribution from the scatterer free dye. (**b**) A cluster and surrounding pumped area for wedges with an angular aperture of $\Theta=36°$. BS, beam splitter; CCD, charge coupled device; OBJ, objective; SLM, spatial optical modulator.

size<1 µm) embedded in a solution of ethylene glycol (refractive index mismatch of 1.2) fabricated as described in Ref. 24. Figure 1a depicts a scheme of the experimental set-up. The pulsed laser (Litron, Warwickshire, UK; 532 nm, 20 mJ pulse energy, repetition frequency 10 Hz), whose spot is shaped by a spatial light modulator (Holoeye, San Diego, CA, USA) in the amplitude configuration (by using the two crossed polarizers P1 and P2), pumps a single titanium dioxide cluster (diameter between 5 µm and 12 µm). The RL emission is collected by a microscope objective and is imaged using a beam splitter in two different image planes. In one of these planes lies a fiber controlled by translators

with nanometric resolution that allows the spatio-spectral map to be measured. In this way, it is possible to scan a magnified (50×) image of the sample and measure the spectra emitted from a single point. The fiber core (50 µm in diameter) collects spectra originating in an area of the sample 1 µm in diameter. The other light path enables the sample to be imaged on a CCD.

The geometrical Θ parameter that is the angular aperture of the lateral wedges (Figure 1b) allows control over the span of the input direction from which the stimulated emission impinges on the cluster; therefore, it selects only the modes that couple efficiently with the wedges. This directional selection allows the user to set the effective number of activated modes in the cluster located in the center of the disc-shaped pumped area.

RESULTS AND DISCUSSION

The first step was isolating the cluster to avoid the influence of other clusters on our measurements. We performed the isolation procedure described in Ref. 24, selecting only 'lonely' clusters (clusters for which the nearest neighbor is more than 800 µm away). In this condition, the spectra measured on neighboring clusters do not show any type of correlation or coupling. Appropriate spatial filtering makes it possible to collect only light emitted from the random lasing cluster, eliminating unwanted contributions from amplified spontaneous emission.[24]

Here, in fact, we are interested in the non-locality generated by modes sharing an individual cluster. Thus, we compared spectra collected at different locations in the same disordered structure because distinct regimes are expected when varying Θ: the interaction is low for small Θ and grows when Θ is increased. Other parameters, such as the size of the pumping wedges and the total pumping volume, do not influence the interaction (see Figures 5 and 12 of Ref. 24). Figure 3 shows five spectra collected at different points of a cluster labeled C1 (Figure 3a for narrow and Figure 3b for wide angular span) and an image of the cluster (inset of Figure 3c) where the crosses mark the positions at which the spectra were collected (with a minimum
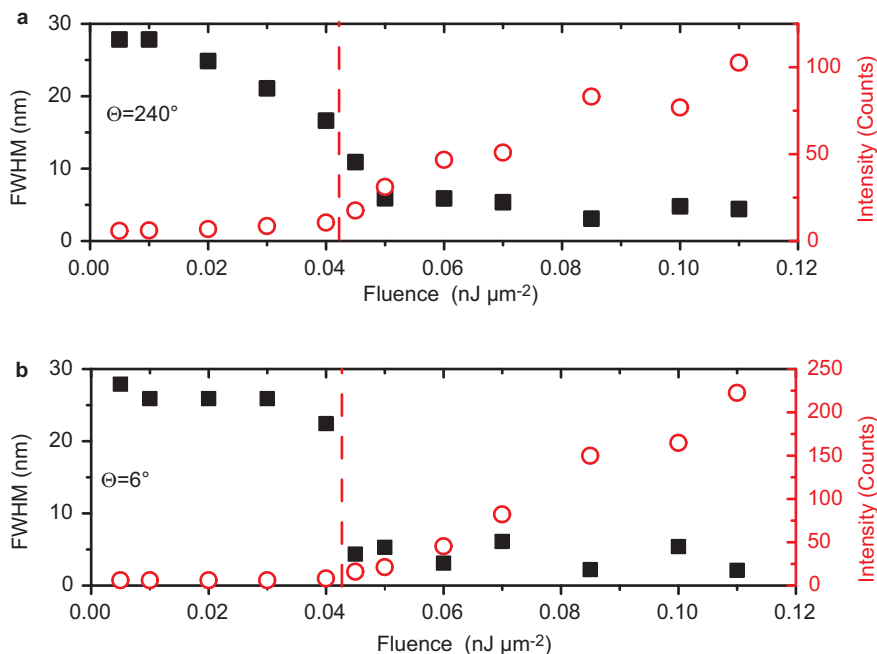

Figure 2 Typical full width at half maximum (left scale) and intensity (right scale) of the light retrieved from a single cluster as a function of the pump intensity for $\Theta=240°$ (**a**) and for $\Theta=6°$ (**b**). The lasing threshold is at the position indicated by the dashed line. FWHM, full width half maximum.

distance between them of 2 μm). When $\Theta = 6°$, the interaction is low, and emission is local, i.e., the spectra display huge variations from point to point. However, when $\Theta = 240°$, the interaction is large, and the spectra are identical throughout the cluster.

The onset of a long-range correlation may be quantified by the overlap Q of the intensity spectra, $I_a(\lambda)$ and $I_b(\lambda)$, collected at different positions a and b defined as $Q_{a,b} = \int I_a(\lambda) I_b(\lambda) d\lambda$ (subject to a normalization condition $Q_{a,a} = Q_{b,b} = 1$). A value of Q close to unity is retrieved for almost identical spectra, while values close to 0 represent distinct emissions from various points. Figure 3c shows the average $Q = <Q> (\Theta)$ (the average is taken over the $N(N-1)/2$ possible pairs among the $N = 5$ considered points) and demonstrates that the correlation between spectra at different positions increases with Θ. A key point is that the increment of Q is not due merely to an average smoothing of the envelope of the spectrum but also includes the persistence of 'small features' (some examples are marked with asterisks in Figure 3b) present in all the considered positions that should not be mistaken for noise. These small features have been previously noticed in earlier experiments, both in titanium dioxide[23] and in zinc oxide microclusters[20] and thin layers.[21]

This measurement is the first direct experimental connection between the strong nonlinear interaction[13] and the appearance of such spectral features. This collective regime can be described by a spatially-dependent Gross–Pitaevskii (GP) equation, making it possible to classify the reported phenomenon as a form of 'condensation'[17] of the localized modes into a single wavefunction (in a dissipative system).

The presented results may be interpreted as follows: the response at wavelength λ_1 can excite the other modes and force them to oscillate at λ_1, i.e., at a frequency different from their natural one. Hence, a localized vibration at λ_1 grows, involving all the modes in neighboring (spatial) regions. However, lossy (or scarcely pumped) modes are not able to retain energy at frequencies far from their fundamental resonances (small Θ regime). On the contrary, when increasing Θ, modes at any point in the structure can sustain oscillations at any frequency,

and as they are all coupled, they synchronize, resulting in large-scale coherent emission. This process is to be compared with other forms of recently reported examples of condensation processes in nonlinear optics,[29–31] and extends previously reported investigations to the spatial domain.[28]

To provide a model for the reported phenomena, we describe the electric field E as a mode superposition written as

$$E = \sum_{j=1,N} \psi_j(\mathbf{x} - \mathbf{x}_j) a_j(t) \exp(-i\omega_j t) \qquad (1)$$

where $\psi_j(\mathbf{x} - \mathbf{x}_j)$ is the wavefunction of the mode centered at position $\mathbf{x}_j$.[32] Note that E and ψ can be vector-valued functions.

As we want to model a continuous distribution of modes, we consider the limit in which $\mathbf{x}_j$ is a continuous variable (many modes are excited and dwell in nearby positions) by introducing the function

$$\psi(\mathbf{x}, t) = \sum_j \delta(\mathbf{x} - \mathbf{x}_j) a_j(t) \qquad (2)$$

which corresponds to taking $a_j(t) = a(t; \mathbf{x}_j)$ and is analogous to the introduction of a continuous particle density, starting from the discrete positions of particles in the theory of liquids.[33]

As $|a_i|^2$ gives the energy of mode i located in $\mathbf{x}_i$, $|\psi(\mathbf{x})|^2$ gives the energy distribution in the system. All the modes are assumed to have the same frequencies ω_0. The small frequency differences can be embedded in the time-dependent $a_j(t)$, which corresponds to letting $a_j \rightarrow a_j \exp[-i(\omega_0 - \omega_i)t]$. The coupled mode equations[23,34,35] are written as:

$$\frac{da_i}{dt} \psi_i(\mathbf{x} - \mathbf{x}_i) = \sum_j K_{ij} \psi_j(\mathbf{x} - \mathbf{x}_j) a_j(t) + \text{nonlinear part} \qquad (3)$$

The coupling coefficients K_{ij} are, in general, complex valued and account for the self-gain/loss coefficient and the detuning $(\omega_0 - \omega_i)$ for the $i = j$ term $(K_S \equiv K_{ii})$, and for the cross-coupling between the modes
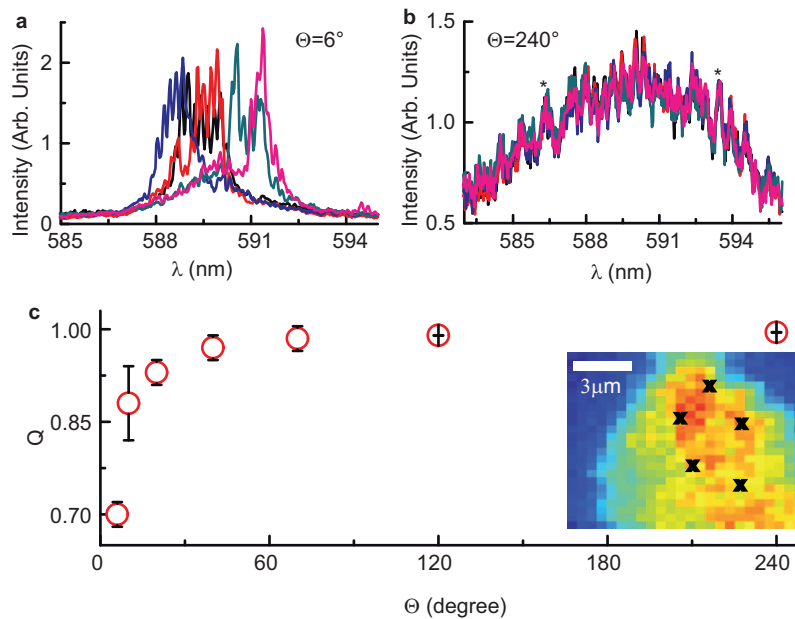

Figure 3 Sample C1: (**a**) spectra (average over 25 shots) collected at five different points for $\Theta = 6°$ and (**b**) $\Theta = 240°$. Both measurements were performed with an input fluence of 0.15 nJ μm^{-2}. (**c**) Average mode overlap Q versus Θ (error bar represents the standard deviation). The inset shows an image of the cluster obtained by fiber scanning. The crosses represent the points where the spectra in (**a**) and (**b**) were collected.

4

$(K_x \equiv K_{ij})$ for $i \neq j$. For the sake of simplicity, we take K_s and K_x independent of the mode index; they represent the average disorder values over the modes, as we are interested in deriving an average equation. Projecting over the state $\psi_i(\mathbf{x} - \mathbf{x}_i)$, one can write

$$\frac{\mathrm{d}a_i}{\mathrm{d}t} = \sum_j \kappa(\mathbf{x}_i - \mathbf{x}_j)a_j(t) + \text{nonlinear part} \qquad (4)$$

where the coupling coefficients are, in general, dependent on the distance between modes. For a cluster size on the order of 10 wavelengths in each direction, with a volume average refractive index $n \cong 2$, we conservatively expect a mode number that is approximately 1000, and hence a continuous limit can be considered as a first-order approximation. In this limit, Equation (4) corresponds ($\mathbf{x}_i \rightarrow \mathbf{x}, \mathbf{x}_j \rightarrow \mathbf{y}$) to

$$\frac{\partial \psi(\mathbf{x},t)}{\partial t} = \int \kappa(\mathbf{x} - \mathbf{y})\psi(\mathbf{y},t)\mathrm{d}\mathbf{y} + \text{nonlinear part} \qquad (5)$$

where $\kappa(\mathbf{x} - \mathbf{y})$ models the coupling between two field values at $\mathbf{x}$ and $\mathbf{y}$ and therefore, describes the inherent non-locality due to the finite spatial extension of the modes and their mutual coupling (open cavity regime, otherwise, the modes are orthogonal). In the weakly non-local limit, $\kappa(\mathbf{x})$ is localized over a spatial extension much smaller than the sample size and of the order of the mode localization length; its Fourier transform $\check{\kappa}(K)$ can be expanded around $\mathbf{k}=0$, i.e., $\check{\kappa}(\mathbf{k}) = k_0 - (k_2/2)\mathbf{k} \cdot \mathbf{k}$, which, in the spatial domain, gives

$$\frac{\partial \psi(\mathbf{x},t)}{\partial t} = k_0 \psi(\mathbf{x},t) + \frac{k_2}{2}\nabla^2 \psi(\mathbf{x},t) + \text{nonlinear part} \qquad (6)$$

where k_0 accounts for the local gain and k_2 is the linear non-locality coefficient. Note that in general, Equation (6) holds in 1, 2 and 3 spatial dimensions. The nonlinear part is, in general, a superposition of the mode-profiles and, at the lowest order, can be written as

$$\iiint \chi(\mathbf{x} - \mathbf{x}_1, \mathbf{x} - \mathbf{x}_2, \mathbf{x} - \mathbf{x}_3)\psi(\mathbf{x}_1)^*\psi(\mathbf{x}_2)\psi(\mathbf{x}_3)\mathrm{d}\mathbf{x}_1\mathrm{d}\mathbf{x}_2\mathrm{d}\mathbf{x}_3 \quad (7)$$

with χ as the nonlinear and non-local kernel function.

For localized modes, the nonlinear cross-correlation between the fields is expected to be small (as the power of the fields decays faster than the fields for an exponential localization), and the non-locality in the linear part dominant; hence, the nonlinear term can be treated in the local limit, i.e.,

$$\chi(\mathbf{x} - \mathbf{x}_1, \mathbf{x} - \mathbf{x}_2, \mathbf{x} - \mathbf{x}_3) = \chi\delta(\mathbf{x} - \mathbf{x}_1)\delta(\mathbf{x} - \mathbf{x}_2)\delta(\mathbf{x} - \mathbf{x}_3) \qquad (8)$$

so that the final equation for the condensed wave function reads

$$\frac{\partial \psi(\mathbf{x},t)}{\partial t} = k_0 \psi(\mathbf{x},t) + \frac{k_2}{2}\nabla^2 \psi(\mathbf{x},t) - |\chi||\psi(\mathbf{x},t)|^2\psi(\mathbf{x},t) \qquad (9)$$

which is the dissipative counterpart of the spatially dependent GP equation, or the Ginzburg–Landau equation with external potential;[10] in the presence of pumping, $k_0 > 0$ and $\chi < 0$ for gain saturation. The fact that we are dealing with a finite cavity can be handled phenomenologically by adding an external potential $V(\mathbf{x})$ that models very large losses (ideally infinite) at a size comparable with the spatial extension of the cluster; this addition forces the solution to be localized in the cluster. The spatial extension of the potential is used as a fitting parameter below.

$$\frac{\partial \psi(\mathbf{x},t)}{\partial t} =$$
$$k_0 \psi(\mathbf{x},t) + \frac{k_2}{2}\nabla^2 \psi(\mathbf{x},t) - V(\mathbf{x})\psi(\mathbf{x},t) - |\chi||\psi(\mathbf{x},t)|^2\psi(\mathbf{x},t) \qquad (10)$$

$V(\mathbf{x})$ can be approximated as finite inside the cluster and infinite elsewhere, so that the field is localized inside the scattering structure with 'infinite losses' outside.

In the stationary regime, $\partial_t = 0$, and Equation (10) corresponds to the time-independent GP equation, providing a form of spatial condensation.[31] Thus, the system considered here shows an evident similarity to the case of ultra-cold atoms for which the transition to the condensed state is triggered by increasing particle density, which in our experiments corresponds to the number of activated modes.

We stress that recently, the problem of light condensation has been discussed by several authors, either with reference to dissipative systems (as lasers)[17,34] or Hamiltonian dynamics;[36–38] the validity of a GP-like (or purely real Ginzburg–Landau) equation to describe the spatial distribution of energy in experiments casts new light on the investigation of these effects, for which further theoretical work is needed and will be reported elsewhere.

A further analogy with matter wave theory can be found in the energy behavior of the collective regime (large Θ configuration). If the potential is approximated with a parabola at low pumping energies, Equation (10) predicts a Gaussian distribution of the intensity. However, for high energies, the kinetic term (the Laplace operator) may be neglected due to the flatter distribution of the intensity. This option leads to the well-known Thomas–Fermi approximation, in which the intensity distribution can be written inside the cluster as

$$|\psi(\mathbf{x})|^2 = \frac{k_0 - V(\mathbf{x})}{|\chi|} \qquad (11)$$

with $k_0 > V(\mathbf{x})$ and

$$|\psi(\mathbf{x})|^2 = 0 \qquad (12)$$

outside the cluster. In Figure 4, we show the numerical solutions of Equation (10) and compare them with the experimental results, with qualitative agreement.

This set of approximations predicts a flattened distribution of the particle density (the light intensity in RLs) inside the potential box (the scattering cluster) when the pumping intensity is increased,[39] and a Gaussian one at low energies. To test this prediction, we studied experimentally the distribution of intensity in the 'many modes' (large Θ) configuration. Specifically, we measured the spatial pattern as a function of the pump fluence for $\Theta = 240^\circ$ for a cluster named C2: we scanned the fiber along the x direction while keeping the y coordinate fixed, thus probing the middle section of the sample.

The results reported in Figure 4 show the intensity distribution for an input pump fluence on the sample of 0.07 nJ μm^{-2} (Figure 4a) and 0.15 nJ μm^{-2} (Figure 4b). These results are presented alongside the numerical solution of the GP equation obtained by a pseudo-spectral Newton–Raphson iterative technique[40] when considering a random Gaussian potential superimposed on a parabolic deterministic component (details will be given elsewhere). Figure 4a reports the linear (low energy) solution, while Figure 4b reports the nonlinear (high energy) solution. Numerical solutions have been found using a one-dimensional version of Equation (9); specifically, the spatial scale of the potential is used as a fitting parameter by using a parabolic approximation with a coefficient to model the size of the system. The energy of the pump is also a fitting parameter.

To further characterize this effect, we measured the localization length Ω of the intensity distribution, which is defined starting from the inverse participation ratio
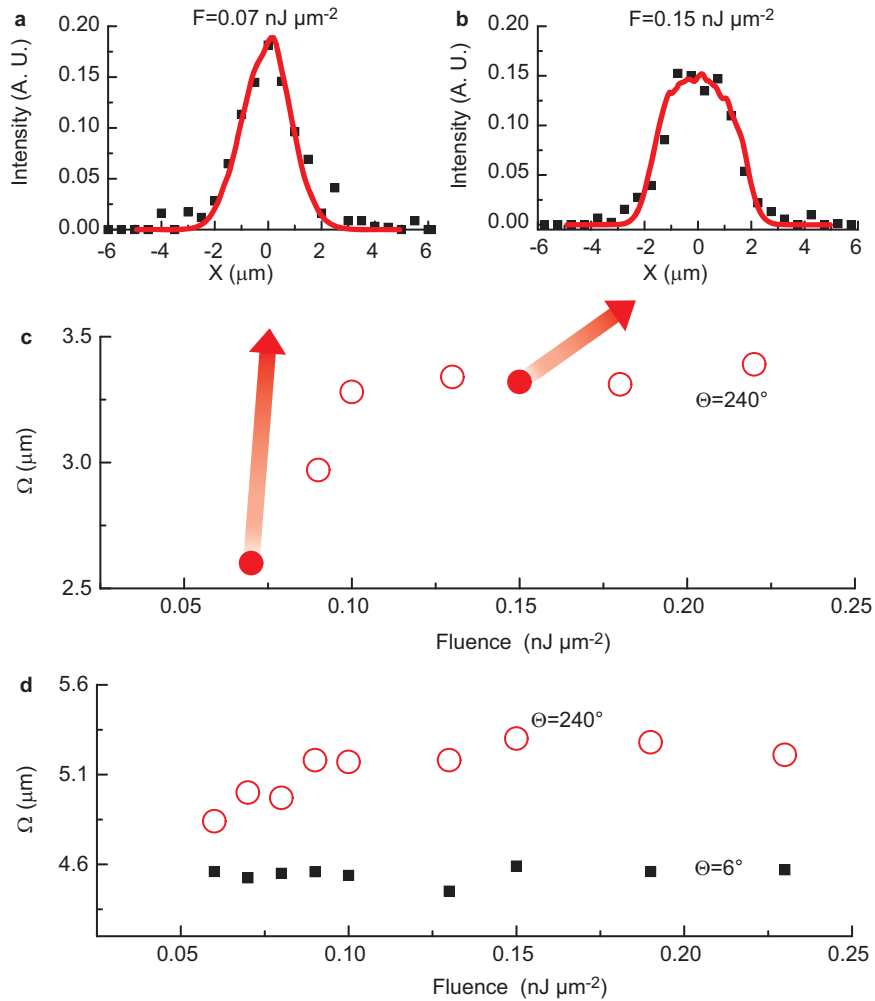
Figure 4 Intensity spatial profile in the middle section of cluster C2 for $\Theta=240°$ and for a fluence of 0.07 nJ μm^{-2} (**a**) and a fluence of 0.15 nJ μm^{-2} (**b**). The continuous line represents the numerical solution of the GP equation in the linear case (**a**) and in the high-energy nonlinear case (**b**). (**c**) Localization length versus fluence for cluster C2 ($\Theta=240°$). Full points correspond to **a** and **b**. (**d**) Localization length versus fluence for cluster C3 for $\Theta=240°$ (open circles) and for $\Theta=6°$ (full squares). GP, Gross–Pitaevskii.

$$P_\lambda \equiv \frac{\int I_\lambda(x,y)^2 \mathrm{d}x\mathrm{d}y}{\left[\int I_\lambda(x,y)\mathrm{d}x\mathrm{d}y\right]^2} \qquad (13)$$

from which

$$\Omega_\lambda \equiv \frac{1}{\sqrt{P_\lambda}} \qquad (14)$$

which is the localization length of the light in the cluster. Figure 4c shows a clear increase of Ω_λ with the pump fluence, as predicted by the model. In Figure 4d, we report a measure of the behavior of Ω_λ for cluster C3 in the presence ($\Theta=240°$) and in the absence ($\Theta=6°$) of interaction. Although small, the increase of Ω in Figure 4d with interaction (and thus non-locality) is clear. When the interaction is suppressed ($\Theta=6°$), the variation of Ω is completely cancelled.

An alternative explanation may be that there are some effects able to modify the intensity distribution. A possibility is given by hole burning, which has been theoretically considered for random lasers.[41,42] Hole burning is due to the presence of standing waves in the cavity, and it is hence expected in both the strongly interacting and the weakly interacting regimes. On the contrary, in our experiments, the spatial smoothing is present only in the interacting case (Figure 4d open circles), confirming that it is interaction that leads to a non-local random laser.

CONCLUSIONS

We demonstrated that in a highly interacting regime, random lasing displays non-local features. In fact, the same fine-featured spectra are found throughout the entire lasing cluster. This result implies that a coherent oscillation distributed over the whole random system is established. Such a finding is accounted for by a model similar to the model used for Bose–Einstein condensates under the Thomas–Fermi approximation, which predicts a stronger confinement of a gas (the RL intensity) inside a potential box (the scattering cluster). The measurements of the spatial intensity distribution of the collective RL as a function of energy confirm that all the observed phenomena are a result of the inter-mode coupling and bring new evidence to the understanding of the fundamental properties of light in random optical cavities and of condensation-like phenomena in a dissipative system. Future investigations may involve studies performed as a function of the refractive index mismatch.

1   Litvak AG, Mironov VA, Fraiman GM, Yunakovskii AD. Thermal self-effect of wave beams in a plasma with a nonlocal nonlinearity. *Sov J Plasma Phys* 1975; **1**: 31–37.
2   Pecseli HL, Rasmussen JJ. Nonlinear electron waves in strongly magnetized plasmas. *Plasma Phys* 1980; **22**: 421–438.
3   Klaers J, Schmitt J, Damm T, Vewinger F, Weitz M. Bose Einstein condensation of paraxial light. *Appl Phys B* 2011; **105**: 17–33.
4   Conti C, Peccianti M, Assanto G. Route to nonlocality and observation of accessible solitons. *Phys Rev Lett* 2003; **91**: 073901.
5   Rotschild C, Schwartz T, Cohen O, Segev M. Incoherent spatial solitons in effectively instantaneous nonlinear media. *Nat Photon* 2008; **2**: 371–376.
6   Akhmediev NN, Lederer MJ, Luther-Davies B. Exact localized solution for nonconservative systems with delayed nonlinear response. *Phys Rev E* 1998; **57**: 3664–3667.
7   Duree GC, Shultz JL, Salamo GJ, Segev M. Observation of self-trapping of an optical beam due to the photorefractive effect. *Phys Rev Lett* 1993; **71**: 533–536.
8   Folli V, Conti C. Anderson localization in nonlocal nonlinear media. *Opt Lett* 2012; **37**: 332–334.
9   Trillo S, Torruealls W. (eds). *Spatial Solitons*. Berlin: Springer-Verlag; 2001.
10 Kivshar YS, Agrawal GP. *Optical Solitons*. New York: Academic Press; 2003.
11 Wiersma DS. The physics and applications of random lasers. *Nat Phys* 2008; **4**: 359–367.
12 Conti C, Leuzzi L. Complexity of waves in nonlinear disordered media. *Phys Rev B* 2011; **83**: 134204.
13 Türeci HE, Ge L, Rotter S, Stone AD. Strong interactions in multimode random lasers. *Science* 2008; **320**: 643–646.
14 Florescu L, John S. Photon statistics and coherence in light emission from a random laser. *Phys Rev Lett* 2004; **93**: 013602.
15 Cao H, Xu JY, Zhang DZ, Chang S, Ho ST *et al*. Spatial confinement of laser light in active random media. *Phys Rev Lett* 2000; **84**: 5584–5587.
16 Turitsyn SK, Babin SA, El-Taher AE, Harper P, Churkin DV *et al*. Random distributed feedback fiber laser. *Nat Photon* 2010; **4**: 231–235.
17 Conti C, Leonetti M, Fratalocchi A, Angelani L, Ruocco G. Condensation in disordered lasers: theory, 3d+1 simulations, and experiments. *Phys Rev Lett* 2008; **101**: 143901.
18 Andreasen J, Asatryan AA, Botten LC, Byrne MA, Cao H *et al*. Modes of random lasers. *Adv Opt Photon* 2011; **3**: 88–127.
19 van der Molen KL, Tjerkstra RW, Mosk AP, Lagendijk A. Spatial extent of random laser modes. *Phys Rev Lett* 2007; **98**: 143901.
20 Fallert J, Dietz RJ, Sartor J, Schneider D, Klingshirn C *et al*. Co-existence of strongly and weakly localized random laser modes. *Nat Photon* 2009; **3**: 279–282.
21 Cao H, Zhao YG, Ong HC, Chang RP. Far-field characteristics of random lasers. *Phys Rev B* 1999; **59**: 15107–15111.
22 Tiwari AK, Uppu R, Mujumdar S. Frequency behavior of coherent random lasing in diffusive resonant media. *Photon Nanostruct Fundam Appl* 2012; **10**: 416–422.
23 Leonetti M, Conti C, Lopez C. The mode-locking transition of random lasers. *Nat Photon* 2011; **5**: 615–617.
24 Leonetti M, Conti C, López C. Random laser tailored by directional stimulated emission. *Phys Rev A* 2012; **85**: 043841.
25 Leonetti M, Conti C, Lopez C. Tunable degree of localization in random lasers with controlled interaction. *Appl Phys Lett* 2012; **101**: 051104.
26 Cao H, Zhao YG, Ho ST, Seeling EW, Wang QH *et al*. Random laser action in semiconductor powder. *Phys Rev Lett* 1999; **82**: 2278–2281.
27 Lawandy NM, Balachandran RM, Gomes AS, Sauvain E. Laser action in strongly scattering media. *Nature* 1994; **368**: 436–438.
28 Leonetti M, Conti C. Haus/Gross–Pitaevskii equation for random lasers. *J Opt Soc Am B* 2010; **27**: 1446–1451.
29 Weill R, Levit B, Bekker A, Gat O, Fischer B. Laser light condensate: experimental demonstration of light-mode condensation in actively mode locked laser. *Opt Express* 2010; **18**: 16520–16525.
30 Connaughton C, Josserand C, Picozzi A, Pomeau Y, Rica S. Condensation of classical nonlinear waves. *Phys Rev Lett* 2005; **95**: 263901.
31 Sun C, Jia S, Barsi C, Rica S, Picozzi A *et al*. Observation of the kinetic condensation of classical waves. *Nat Phys* 2012; **8**: 471–475.
32 Hansen JP, McDonald IR. *Theory of Simple Liquids*. 2nd ed. London: Academic Press; 1986.
33 Hackenbroich G, Viviescas C, Haake F. Quantum statistics of overlapping modes in open resonators. *Phys Rev A* 2003; **68**: 063805.
34 Haus H. Mode locking of lasers. *IEEE J Select Top Quantum Electron* 2000; **6**: 1173–1185.
35 Angelani L, Conti C, Ruocco G, Zamponi F. Glassy behavior of light in random lasers. *Phys Rev B* 2006; **74**: 104207–104223.
36 Fischer B, Weill R. When does single-mode lasing become a condensation phenomenon? *Opt. Express* 2012; **20**: 26704–26713.
37 Michel C, Haelterman M, Suret P, Randoux S, Kaiser R *et al*. Thermalization and condensation in an incoherently pumped passive optical cavity. *Phys Rev A* 2011; **84**: 033848.
38 Garnier J, Lisak M, Picozzi A. Toward a wave turbulence formulation of statistical nonlinear optics. *J. Opt. Soc. Am. B* 2012; **29**: 2229–2242.
39 Dalfovo F, Giorgini S, Pitaevskii L, Stringari S. Theory of Bose–Einstein condensation in trapped gases. *Rev Mod Phys* 1999; **71**: 463–512.
40 Conti C. Solitonization of the Anderson localization. *Phys Rev A* 2012; **86**: 061801.
41 Tureci H, Ge L, Rotter S, Stone AD. Strong interactions in multimode random lasers. *Science* 2008; **320**: 643–646.
42 Vanneste C, Sebbah P. Selective excitation of localized modes in active random media. *Phys Rev Lett* 2001; **87**: 183903.